Wu *et al. Virology Journal* (2025) 22:138
https://doi.org/10.1186/s12985-025-02759-x

Virology Journal

RESEARCH Open Access

Inhibitory effect of Alantolactone against varicella-zoster virus in vitro

Xinna Wu[1†], Yunchuang Chang[2†], Chengcheng Kong[3], Zhiwei Ding[2], Dongli Pan[4], Ping Lin[3,5*], Sanying Wang[2*] and Genxiang Mao[1,2*]

Abstract

Background Varicella-zoster virus (VZV), a member of the α-herpesvirus family, is known for causing two distinct diseases: chickenpox (varicella) during the primary infection and shingles (zoster) due to reactivation of the virus later in life. Although there are vaccines available to prevent VZV infection, it is still not universally effective, and antiviral treatments for VZV are limited and may come with significant side effects. Thus, development of novel therapeutics is urgently needed.

Methods We identified a naturally occurring Alantolactone (ALT) that inhibited replication of recombinant VZV in human diploid fibroblast (WI-38 cells) and Adult Retinal Pigment Epithelial cell line-19 (ARPE-19 cells) through Western blotting, qPCR and plaque assays. Subsequently, we explored the mechanism underlying the anti-VZV activity of ALT using time-of-addition experiments and transcriptomic analyses.

Results A screening model was established for anti-VZV compounds, and we screened ALT was with good anti-VZV efficacy. Our findings revealed that ALT alleviated cytopathic changes, reduced viral titres, and inhibited the expression of viral genes and proteins in WI-38 cells and ARPE-19 cells. Furthermore, our data showed that ALT inhibited VZV infection in intracellular viral replication. Finally, multiple inflammatory pathways were involved in the antiviral role of ALT, and IL-6 was one of the most critical hub genes.

Conclusion Together, our findings identify ALT as an anti-VZV agent that may prove useful in the treatment of VZV replication.

Keywords Alantolactone, Varicella-zoster virus, Screening model, IL-6

†Xinna Wu and Yunchuang Chang contributed equally to this work.

*Correspondence:
Ping Lin
Yjlp1@163.com
Sanying Wang
sanyingwang309@126.com
Genxiang Mao
maogenxiang@zju.edu.cn
[1]Affiliated Zhejiang Hospital, Zhejiang University School of Medicine, No.1229 Gudun Road, Xihu District, Hangzhou 310030, China
[2]Zhejiang Key Laboratory of Geriatrics and Geriatrics Institute of Zhejiang Province, Zhejiang Hospital, No.1229 Gudun Road, Xihu District, Hangzhou 310030, China
[3]Geriatric Department of the 3rd Hospital of Hangzhou, Hangzhou 310009, China
[4]Department of Medical Microbiology and Parasitology, Zhejiang University School of Medicine, Hangzhou 310030, China
[5]Hangzhou Third People's Hospital, No.38, Xihu Avenue, Shangcheng District, Hangzhou, Email, China

Introduction

Herpesviruses are ubiquitous, double-stranded DNA, enveloped viruses that establish lifelong infections and cause a range of diseases [1, 2]. Varicella-zoster virus (VZV), also known as human a herpesvirus 3, is a highly contagious, neurotropic virus. There are no animal reservoirs, and it naturally infects only humans with its main targets being T lymphocytes, ganglia, and epithelial cells [3]. The VZV virion structure is composed of four major elements: core, nucleocapsid, tegument, and envelope. The icosahedral nucleocapsid surrounds the core containing a linear double-stranded DNA genome of 125 kb encoding 71 open reading frames (ORF) [4, 5]. After entry into the host cell through receptor-mediated fusion or endocytosis, the nucleocapsid is transported into the nucleus with the aid of tegument proteins, where sequential expression of immediate early (IE), early (E) and late (L) lytic genes and viral DNA replication occur [4, 5]. IE genes regulate the expression of early and late genes. The E genes encode proteins for viral DNA replication while L genes encode structural constituents of the virion, including glycoproteins and nucleocapsid proteins [6, 7].

VZV is prevalent worldwide and estimated to infect more than 95% of the global population [8]. Primary infection of VZV causes a diffuse rash of varicella (chickenpox) after which latent infection is established in the sensory nerve ganglia [3]. The latent period is variable, and VZV is often reactivated to cause herpes zoster when cell-mediated immunity declines due to aging or immunosuppression [4, 9]. Herpes zoster is typically characterized by co-occurrence of segmental rash and segmental pain that lasts for more than three months, which is known as postherpetic neuralgia (PHN) [10]. PHN is the most common complication of the disease and is age-related [11, 12]. In addition, herpes zoster is associated with various ophthalmic and neurological complications [4, 9].

Current antiviral drugs for the therapy of VZV-associated diseases include acyclovir, valacyclovir, famciclovir/penciclovir, and foscarnet that target viral DNA polymerase [6, 13–15]. These licensed drugs are used in combination with corticosteroids for against inflammation and narcotics for relieving from pain during treatment of VZV infection [4]. Although these anti-VZV drugs are highly effective, more concerted efforts to develop novel therapeutic strategies for VZV-associated diseases are necessary due to the emergence of drug resistance and side effects of available antiviral agents [13, 16, 17].

Natural compounds are valuable sources of drug development. Certain plant-derived chemical compounds have been determined to possess anti-VZV activity [14, 18–21]. Alantolactone (ALT) is a natural sesquiterpene lactone isolated from *Inula helenium* and is known to have many biological properties [22, 23], including anti-inflammatory [24–27], antitumor [28–30], antimicrobial [25, 31, 32], as well as neuroprotective activities [33, 34]. In addition, this compound has been shown previously to inhibit herpes simplex virus 1 (HSV-1) [35], indicating the antiviral activity of ALT. In this study, we identified ALT as a candidate compound with anti-VZV efficacy in *vitro.*

Materials and methods

Agent

All the tested compounds mentioned in the current study were purchased from Shanghai Standard Technology Co., Ltd. (Shanghai, China) and dissolved in dimethyl sulfoxide (DMSO) for a stock solution of 10mM. Foscarnet (FOS) was purchased from Sigma-Aldrich (St. Louis, MO, USA). Dulbecco's modified Eagle's medium (DMEM), foetal bovine serum (FBS), 100 × penicillin-streptomycin solution, and 0.25% trypsin-EDTA were purchased from Gibco-BRL Life Technologies (Grand Island, NY, USA). DMEM/F12 was purchased from Cell-Max (Beijing, China).

Cell culture and virus

Human diploid lung fibroblasts (WI-38) and human retinal pigment epithelial (RPE) cells are two classical cell lines that can be infected by VZV [10, 36, 37]. Human diploid fibroblasts (WI-38 cells) and Adult Retinal Pigment Epithelial cell line-19 (ARPE-19 cells) were obtained from the American Tissue Culture Collection (ATCC, Manassas, VA, USA). Cells were cultured in DMEM containing 10% FBS and 100 U/ml of penicillin and streptomycin solution.

In the current studies, a recombinant VZV was used which was from the lab of Hua Zhu. This recombinant VZV had an insertion of the GFP gene in the viral genome [38]. Cell-free VZV was prepared by following a previously published method [37, 39], with some modifications. Briefly, ARPE-19 cells were infected with VZV and when an extensive cytopathic effect was observed (3–4 days), the cells were scraped in PBS-sucrose-glutamate-serum (PSGC) buffer [37]. The cells and buffer were homogenized with a Dounce homogenizer (Wheaton, Millville, NJ) on ice for 3 min and treated with RNase A. Cell-free VZV was aliquoted and stored in liquid nitrogen [39]. The final titer of the cell-free virus pool used in this study was 2×10^5 pfu/ml.

VZV infection and compounds treatment

The cells were mock-infected or infected with VZV (MOI = 0.04) for 1 h at 37 °C. Then, the inoculum was discarded, and the cells were washed and incubated with fresh culture medium with 10% FBS in the absence or the presence of compounds. FOS (100 μg/mL) was used as a positive-drug control. 0.1% DMSO solution (V/V) was

used as vehicle control. Cells were pretreated with tested compounds or FOS 2 h before virus inoculation and cultured for indicated time before harvest.

Preliminary screening of anti-VZV compounds

ARPE-19 cells were seeded at a density of $5 \times 10^4/cm^2$ in 96-well black clear bottom plates (Cellvis, Hangzhou, Zhejiang). When the cell density reached 80%, ARPE-19 cells were treated with tested compounds(10μM) and infected with VZV(MOI = 0.04) as described above. Mock, DMSO + VZV, and FOS + VZV groups were set up for each plate of screening compounds. Each group was set up with three replicates. The fluorescence signal of GFP was observed using a Zeiss microscope (Axio Vert. A1). The fluorescence intensity of GFP in 96-well black clear bottom plates was detected at the indicated time using the Tecan Spark™ (Swiss), with the excitation and emission wavelengths set at 485 nm and 535 nm, respectively. The exploration process for the conditions of the above-mentioned screening model (including the final concentration of DMSO, MOI, and dpi) was provided in the supplementary materials (Figure S1). The inhibition efficacy against VZV was calculated by mean fluorescence intensity, using the following equation:

$$\begin{aligned} &Inhibitive\ efficacy\ \% \\ &= [1 - (Mean_{Test+VZV} - Mean_{Mock}) \\ &/(Mean_{DMSO+VZV} - Mean_{Mock})] \times 100\% \end{aligned}$$

CCK-8 assay

The effect of compounds on cell viability was determined by CCK-8 assays (Abclonal, Wuhan, China). Briefly, cells were seeded in 96-well plates at a density of 5×10^3 cells/well and incubated at 37 °C. Subsequently, culture medium containing different concentrations of compounds was added and incubated for 4 days. At the predetermined time, 10μL of CCK-8 was added to each well. After incubation for 0.5–1 h at 37 °C, the absorbance was measured using the Tecan Spark™ (Swiss) at 450 nm according to the standard protocol.

Table 1 Primers used for PCR

No.	Gene	Forward primer	Reverse primer
1.	ORF62	TCTCGACTGGCTGGGACTTG	CGCCGCACGCTCTCTTT
2.	ORF68	TAATCAGGGCCGTGGTATC	GGGGGTCTAATTC-GAGTTCATCAA
3.	ORF21	ACAAGGCAGTTTCATTCG	GGTCACTCCCACTTG-TATTCC
4.	GAPDH	CTGTTGCTGTAGCCAAATTCGT	ACCCACTCCTC-
5.	IL-6	CACTGGTCTTTTGGAGTTTGAG	CACCTTTGAC GGACTTTTGTACT-CATCTGCAC

Plaque assay

Confluent ARPE-19 cell monolayers in twelve-well plates were incubated with 100-fold serial dilutions of VZV-infected cell suspension at 37 °C for 1 h. Then after removal of the inoculum, cells were washed and overlaid with Methylcellulose culture-medium(5% [wt/vol] methylcellulose, 2% FBS, 1% PenStrep). After incubation for 7 days, the cells were fixed with fixing solution and stained with 0.5% crystal violet. The number of plaques was counted, and viral inhibition percentage was calculated using the following formula: viral inhibition ratio (%) = [1-(number of plaques)$_{ALT}$/ (number of plaques)$_{control}$]×100 [40]. The half-maximal inhibitory concentration (IC50) was determined using Graphpad Prism. Nonlinear regression analysis was conducted within GraphPad Prism by selecting "Nonlinear regression (curve fit)" and applying the "log(inhibitor) vs. response—Variable slope (four parameters)" model. Constraints were applied, with the "Bottom" parameter set to 0 and the "Top" parameter set to 100. The goodness-of-fit was assessed using the coefficient of determination (R^2), with values exceeding 0.85 indicating a satisfactory fit. The 95% confidence intervals (CIs) for the IC50 values were calculated based on the standard error (SE) of the fit. The datas were rounded to two decimal places.

Western blotting

The cell samples were prepared as described above and lysed in RIPA buffer supplemented with protease and phosphatase inhibitors. Then, 50 μg of protein extract was subjected to SDS–PAGE and transferred to PVDF membranes. The membranes were blocked in 5% nonfat dry milk for 1 h at room temperature and then incubated with primary antibodies overnight at 4 °C. The primary antibodies were: anti-VZV IE62 antibody was purchased from GeneTex (GTX64190, North America); anti-VZV gE antibody was purchased from Abcam(AB272686, Cambridge, England); anti-IL6 antibody was purchased from Proteintech (21865-1-AP, North America); anti-β-Actin antibody, anti-GAPDH antibody and secondary antibodies were purchased from Abclonal (Wuhan, China). The membrane was washed three times in TBST buffer and incubated with secondary antibodies at room temperature for 1 h. Blots were developed using enhanced chemiluminescence reagents.

qPCR

Cell Fast RNA Extraction Kit (ABclonal, Wuhan, China) was used to isolate and purify the total RNA from samples. cDNA was synthesized using Primescript RT Master Mix (Transgen, Beijing, China) following the manufacturer's guidance. qPCR was conducted using 2 × Universal SYBR Green Fast qPCR Mix (ABclonal, Wuhan, China). The gene primers used in this study are

provided in Table 1. The qPCR procedure was as follows: 3 min at 95 °C for initial denaturation, 40 cycles of 5 s at 95 °C and 30 s at 60 °C. Each group was assayed in triplicates ($n = 3$). The difference in viral gene expression between the ALT treatment group and the virus infection alone group was calculated using the $2^{-\triangle\triangle Ct}$ method. First, the housekeeping gene GAPDH was used to normalize the Ct values of all treatment and control samples, i.e., ΔCt = Ct (sample) – Ct (GAPDH). Second, the Ct values of the ALT treatment groups were compared to those of the control samples. ΔΔCt = ΔCt (sample) – ΔCt (control sample). The relative expression of the target gene is represented by $2^{-\triangle\triangle Ct}$.

Time-of-addition experiments

ARPE-19 cells or WI-38 cells were infected with VZV (MOI = 0.04) for 1 h and treated with ALT (10μM) or 0.1%DMSO(V/V) at the indicated time. VZV infection and ALT or DMSO treatment were terminated by discarding the culture medium, followed by washing the cells with PBS and replenishing the fresh medium. In pre cell group, ALT or vehicle was pretreated with the cells for 1 h. ln pre virus group, ALT was incubated with the VZV at 37 °C for 2 h before the drug-virus mixture was added to the cells. In post-infection group, the cells were infected with VZV for 1 h and then the viruses were discarded, followed by washing its host cells with PBS and replenishing fresh medium with ALT. The cell samples of each group were collected at 72 hpi (hours post-infection) for qPCR assay.

Transcriptome RNA sequencing analysis

The WI-38 cells were mock-infected or infected with VZV using a MOI of 0.04 and divided into 3 groups: Mock, DMSO + VZV, ALT + VZV, with 3 replicates in each group. Cellular samples were collected at 3 dpi and total RNA was extracted using TRIzol Reagent (Invitrogen, USA). The quantity and purity of total RNA were analyzed by Bioanalyzer 2100 and RNA 6000 Nano Kit (Agilent, USA), and high-quality RNA samples with RIN number > 7.0 were used to construct a sequencing library. High-throughput sequencing was performed using an Illumina Novaseq™ 6000 system (LC-Bio Technology CO., Ltd., Hangzhou, China) with 150-bp paired-end reads (PE150). Cutadapt and fastqc software (https://github.com/OpenGene/fastp) was used to remove the reads that contained adaptor contamination, low quality bases and undetermined bases with default parameter. HISAT2 (https://ccb.jhu.edu/software/hisat2) was used to map reads to the reference genome of Homo sapiens GRCh38. The mapped reads of each sample were assembled using StringTie (https://ccb.jhu.edu/software/stringtie) with default parameters. Then, all transcriptomes from all samples were merged to reconstruct a comprehensive transcriptome using gffcompare (https://github.com/gpertea/gffcompare/). After the final transcriptome was generated, StringTie and was used to estimate the expression levels of all transcripts. StringTie was used to perform expression level for mRNAs by calculating FPKM. The differentially expressed mRNAs were selected with fold change > 2 or fold change < 0.5 and with parametric F-test comparing nested linear models (p value < 0.05) by R package DESeq2 (https://bioconductor.org/packages/release/bioc/html/edgeR.html). Visual representations was performed using the OmicStudio tools at https://www.omicstudio.cn/tool. The sequencing data have been d eposited in the GEO repository under accession number GSE289362 to ensure compliance with standard practices regarding data availability.

Statistical analysis

Statistical analyzes were performed using GraphPad Prism 9 software (GraphPad Prism, San Diego, CA, USA). All experiment results are represented as the mean ± standard deviation (SD) from at least three independent experiments. Student's t test or one-way analysis of variance (ANOVA) were used for statistical analysis. The difference was considered statistically significant when P-value < 0.05.

Results

VZV replication is inhibited by ALT

In this study, 50 natural compounds (Table S1) were tested and their inhibition efficacy against VZV was calculated as mentioned in Materials and Methods. As shown in Fig. 1A, ALT exhibited an optimal inhibition efficacy (over 50%), suggesting its potential as an antagonist against VZV. Before evaluating the inhibiting effect on VZV, the cytotoxicity of ALT was determined in ARPE-19 cells and WI-38 cells using the CCK-8 assay after 4 days of treatment. We observed that the half-maximal cytotoxicity concentration (CC50) of ALT treatment was 24.27μM in ARPE-19 cells (Fig. 1C) and 25.61μM in WI-38 cells (Fig. 1D), respectively. Concentrations used in subsequent experiments were within safe limits.

Previously, obvious cytopathic effects (CPE) [36, 41]and green fluorescent plaques [38] in VZV-infected cells were observed. As shown in Fig. 1E, ARPE-19 cells infected with VZV alone at an MOI of 0.04 displayed many green fluorescent plaques and typical CPE characterized by enlarged cells with increased granularity at 4dpi, while pretreatment of the cells with 10μM ALT significantly reduced the degree of CPE and the sizes of green fluorescent plaques. In addition to ARPE-19 cells, WI-38 cells were also used as infected cells [39]. WI-38 cells infected with VZV underwent corresponding changes, but the typical CPE of WI-38 cells was characterized by rounded or degenerated cells, usually in an elongated patch. These

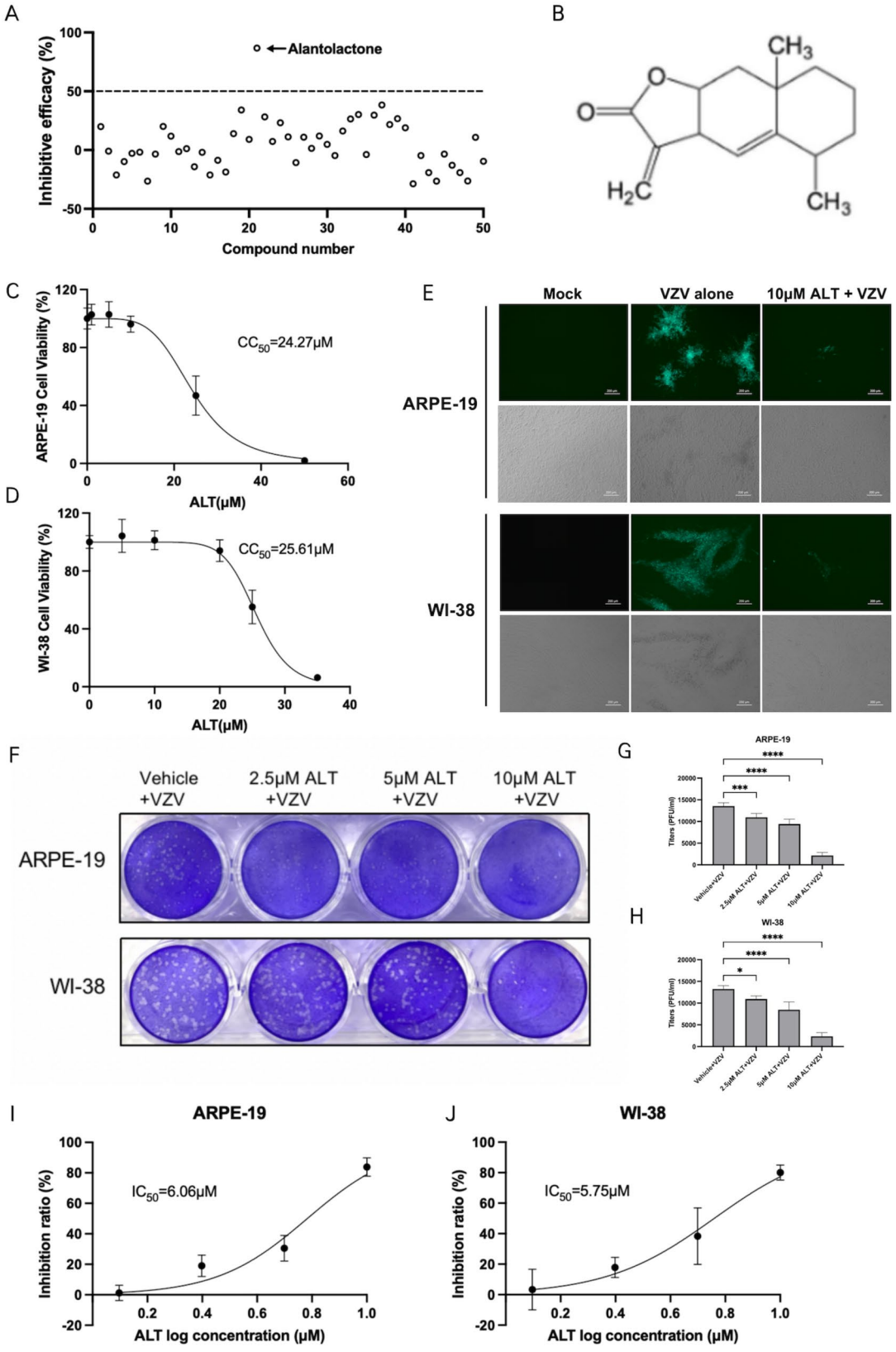

Fig. 1 (See legend on next page.)

(See figure on previous page.)

Fig. 1 ALT inhibited VZV replication in vitro. (**A**) A primary screen of 50 natural compounds against VZV infection at 10μM. Arrow indicated that ALT with optimal inhibition efficacy (86.6%) was selected. (**B**) Chemical structure of alantolactone. (**C**) and (**D**) Cell viability was measured in ARPE and WI-38 cells after being treated with ALT for 4 days. Cells were treated with ALT at the indicated concentrations. Cell viability was analyzed by CCK-8 assays. The half-maximal cytotoxicity concentration (CC50) was determined based on the results of the cell viability assay according to nonlinear trajectory analysis using GraphPad Prism. (**E**) Effects of ALT on morphological changes with or without VZV infection. ARPE-19 and WI-38 cells were infected with VZV at an MOI of 0.04, and typical CPE and green fluorescent plaques were observed at 4 days post infection (dpi). In the ALT treatment group, cells were pretreated with ALT at the indicated concentrations 1 h before VZV infection. (**F**) Plaque assays were performed according to materials and methods. (**G**) and (**H**) VZV virus titers of each group were calculated. The experiments were duplicated at least three times. (**I**) and (**J**) The falf-maximal inhibitory concentration (IC50) was determined based on the results of the Plaque assays according to nonlinear trajectory analysis using GraphPad Prism. *P* values were calculated with one-way ANOVA. ($^{*}P < 0.05$, $^{**}P < 0.01$, $^{***}P < 0.001$, $^{****}P < 0.0001$)

results indicated that ALT could protect the morphological features of the ARPE-19 cells and WI-38 cells infected with VZV and further suggested that ALT might have anti-VZV activity, which is not cell type-specific. To further verify the effect of ALT on VZV replication, the plaque assay was employed. The number of plaques was counted to determine the titers (pfu/ml) via the plaque assay. ALT treatment induced a significant reduction in plaque number, notably at 5μM and 10μM (Fig. 1F-H). The half-maximal inhibitory concentrations (IC50) were determined as 6.06μM (95% CI: 5.39, 6.80μM) for ARPE-19 and 5.75μM (95% CI: 4.90, 6.74μM) for WI-38, respectively (Figs. 1I-J). In conclusion, ALT could suppress VZV infection in host WI-38 cells and ARPE-19 cells.

Preliminary investigation of antiviral mode of action

During the lytic cycle of infection, VZV lytic genes are expressed in a sequential cascade composed of immediate early (IE), early (E), and late (L) genes [4, 5]. To test the effects of ALT on VZV lytic gene expression, we performed RT-qPCR and Western blotting to assess the expression of viral genes and proteins. ARPE-19 cells and WI-38 cells were infected with VZV at an MOI of 0.04, pretreated with DMSO, FOS or ALT. First, the relative transcript levels of ORF62 encoding IE62 (IE), ORF21 (E) and ORF68 encoding glycoprotein E (gE) (L) were analyzed via qRT-PCR at 3 dpi. Compared with the VZV-alone group, the transcript levels of the ORF62, ORF21 and ORF68 were reduced after treatment with ALT both in ARPE-19 cells and WI-38 cells (Fig. 2A and B). The results were consistent with the expression levels of IE62 and gE proteins. Compared with the VZV-alone group, the expression levels of the IE62 and gE proteins were reduced rapidly after treatment with ALT in a concentration-dependent manner (Fig. 2C-H).

The observed decrease in gene and protein expression during the lytic cycle of infection was probably the result of viral infection or replication defects. To expand our knowledge regarding the mode of action of ALT, we performed time-of-addition experiments schematically shown in Fig. 3A. As demonstrated, when media containing DMSO or ALT was premixed with cell-free VZV and incubated at 37°C before VZV infection, there was no significant inhibitory effect on expression of ORF62 compared with the DMSO + VZV group (Fig. 3B). However, when ALT was only pretreated with ARPE-19 cells before VZV infection, ORF62 expression was reduced (Fig. 3B). This implied that ALT may not interact directly with VZV, but rather on cells. In addition, a significant inhibitory effect was observed when ALT was added to the cells only post-infection (Fig. 3B). The outcome on WI-38 cells is similar to the effect seen in ARPE-19 cells (Fig. 3C). These results suggested that ALT inhibited VZV infection in intracellular viral replication.

ALT had a significant inhibitory effect on VZV-induced inflammatory response

To illustrate host cell response to VZV infection and ALT treatment, we used RNA-sequencing in VZV Mock group and VZV treated with DMSO or ALT group to outline their gene expression patterns. The Venn diagram showed that there were 3657 differentially expressed genes (DEGs) between the ALT + VZV and DMSO + VZV groups, 2570 DEGs between the DMSO + VZV and Mock groups, and 1257 genes that overlapped (Fig. 4A). KEGG enrichment analysis of the overlapped DEGs showed that multiple inflammatory pathways, such as the PI3K-Akt signaling pathway and cytokine-cytokine receptor interaction, were significantly enriched (Fig. 4B). Subsequently, interleukin 6 (IL-6) was identified as a hub gene in PPI networks by targeting overlapped genes in these pathways (Fig. 4C). IL-6 is the most typical cytokine associated with inflammation. It plays an important role in host defense by regulating immune and inflammatory responses [42, 43]. qPCR and Western blotting results showed that, compared with the DMSO + VZV group at 3dpi, the ALT + VZV group had considerably lower IL-6 expression at both transcription and protein levels (Fig. 4D-E), which was consistent with the RNA-sequencing results. These findings suggested that ALT had a significant inhibitory effect on VZV-induced inflammatory response.

Discussion

Varicella-zoster virus infection causes severe disease in immunocompromised individuals, especially those with impaired cell-mediated immune responses. VZV infection can develop into disseminated disease, such

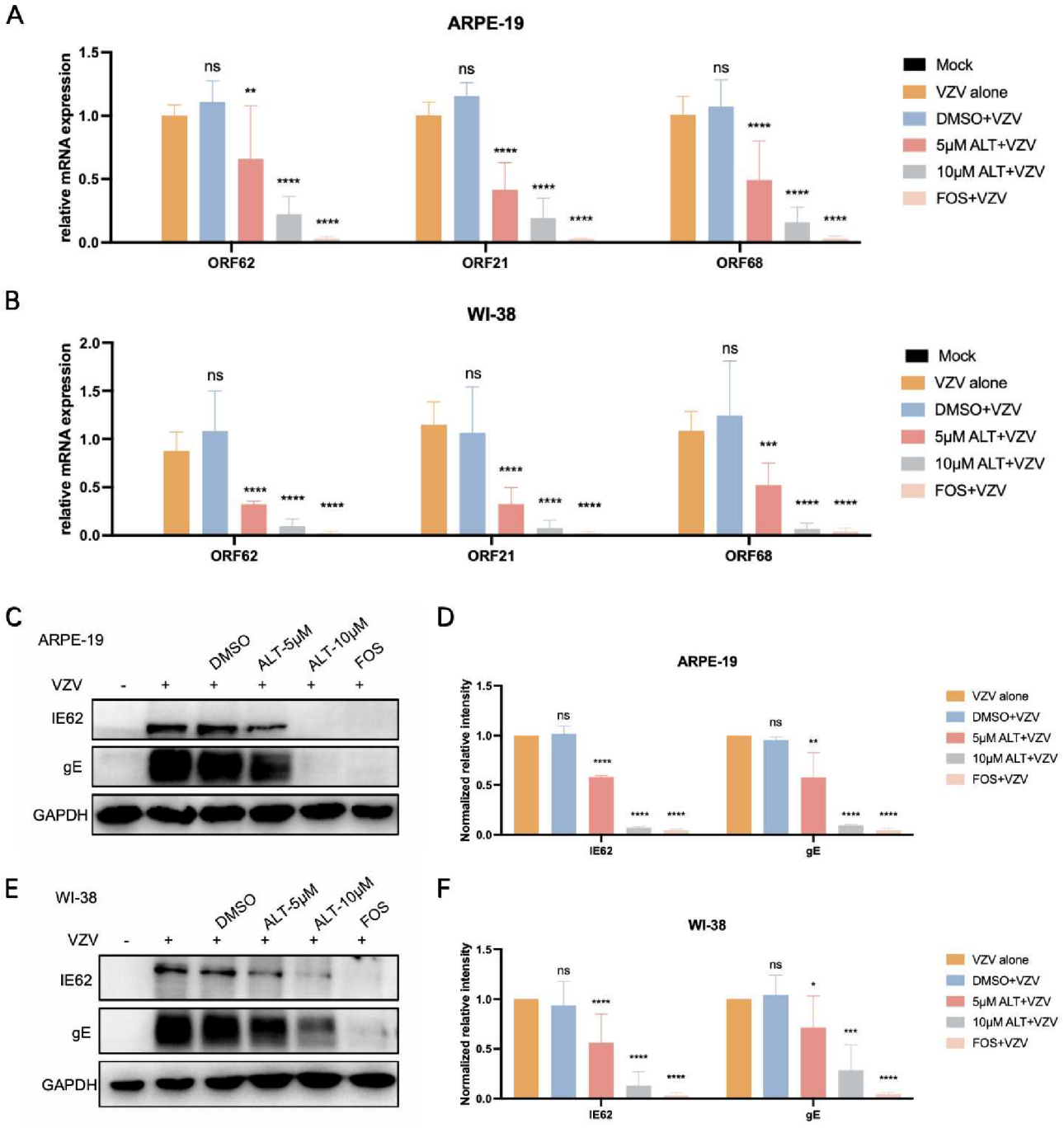

Fig. 2 ALT inhibited lytic gene expression in ARPE-19 and WI-38 cells. (**A**) and (**B**) qPCR analysis of VZV viral gene expression in ARPE-19 and WI-38 cells. Total RNA was isolated at 3 dpi and subjected to qPCR analysis with the primers specific to VZV ORF62, ORF21, and ORF68. Relative RNA expression was normalized to GAPDH in each sample, as described in Materials and methods. The VZV alone group was used as control. (**C**) Expression levels of IE62 and gE in the VZV-infected ARPE-19 cells with or without ALT treatment. ARPE-19 cells were pretreated with ALT (5μM, 10μM) for 2 h before (-1 h) VZV inoculation (MOI of 0.04). Protein expression intensity was analyzed using western blotting at 4 dpi. GAPDH was used as the loading control. Representative images were acquired from three different independent experiments. (**D**) Quantitative analysis of the protein levels of IE62 and gE from three independent experiments. The treatment performed on WI-38 cells was the same as C and D in ARPE-19 cells. The VZV alone group was used as control. (**E**) Expression levels of IE62 and gE in the VZV-infected WI-38 cells with or without ALT treatment. WI-38 cells were pretreated with ALT (5μM, 10μM) for 2 h before (-1 h) VZV inoculation (MOI of 0.04). Protein expression intensity was analyzed using western blotting at 4 dpi. GAPDH was used as the loading control. Representative images were acquired from three different independent experiments. (**F**) Quantitative analysis of the protein levels of IE62 and gE from three independent experiments. The VZV alone group was used as control. P values were calculated with one-way ANOVA. (*$P < 0.05$, **$P < 0.01$, ***$P < 0.001$, ****$P < 0.0001$)

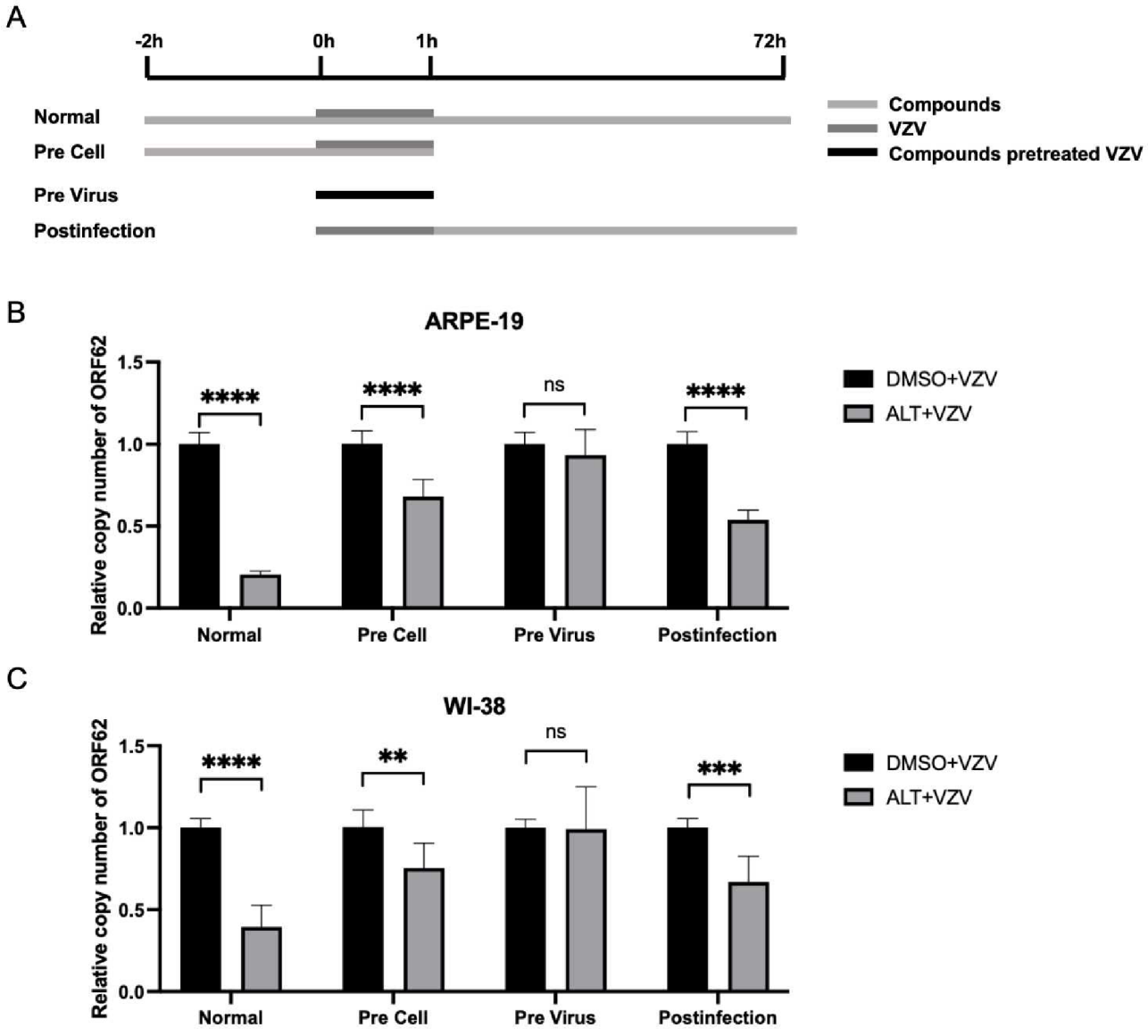

Fig. 3 ALT inhibits VZV infection at certain stages of the viral life cycle. (**A**) Schematic representation of the Time-of-addition experimental design. (**B**-**C**) ARPE-19 or WI-38 cells were treated with 10μM ALT as described in (**A**) and infected with VZV (MOI = 0.04). Intracellular viral DNA was extracted at 72 hpi. The copy numbers of ORF62 gene were measured with the $2^{-\Delta\Delta}$Ct method, the VZV + DMSO group was used as control. The experiments were repeated three times. P values were calculated with Student's t-test. (**$P < 0.01$, ***$P < 0.001$, ****$P < 0.0001$, ns means no significance)

as widespread skin lesions, pneumonia, hepatitis, or encephalitis [6]. Owing to side effects and emergence of resistant VZV strains, limited antiviral drugs are currently available to VZV-associated diseases [13]. Many extracts of natural products have been proven to have antiviral activities [7, 44, 45]. In this study, we found that alantolactone(ALT) possesses optimal anti-VZV properties, which were further confirmed and explored.

Here, GFP was used as a labelling tool for VZV infection, and the infection status was verified by observing green fluorescent plaques. GFP fluorescence intensity correlates with the extent of viral infection, as the intensity and number of fluorescent plaques reflect the number of infected cells and the level of viral replication. Therefore, the fluorescence intensity of GFP can be used to assess viral viability qualitatively or semi-quantitatively. Based on this property, we established a preliminary screening model for anti-VZV compounds (Figure S1), which we utilize to rapidly and easily screen for ALT (Fig. 1A). Although ALT has not been shown to be anti-VZV, it has been shown to be anti-HSV-1 [35], suggesting that this screening model might be meaningful in screening for broad-spectrum anti-herpesvirus drugs.

Human retinal pigment epithelial (RPE) cells or human diploid lung fibroblasts (WI-38) are the most often used cell lines that VZV can infect [10, 36, 37, 39, 46]. In

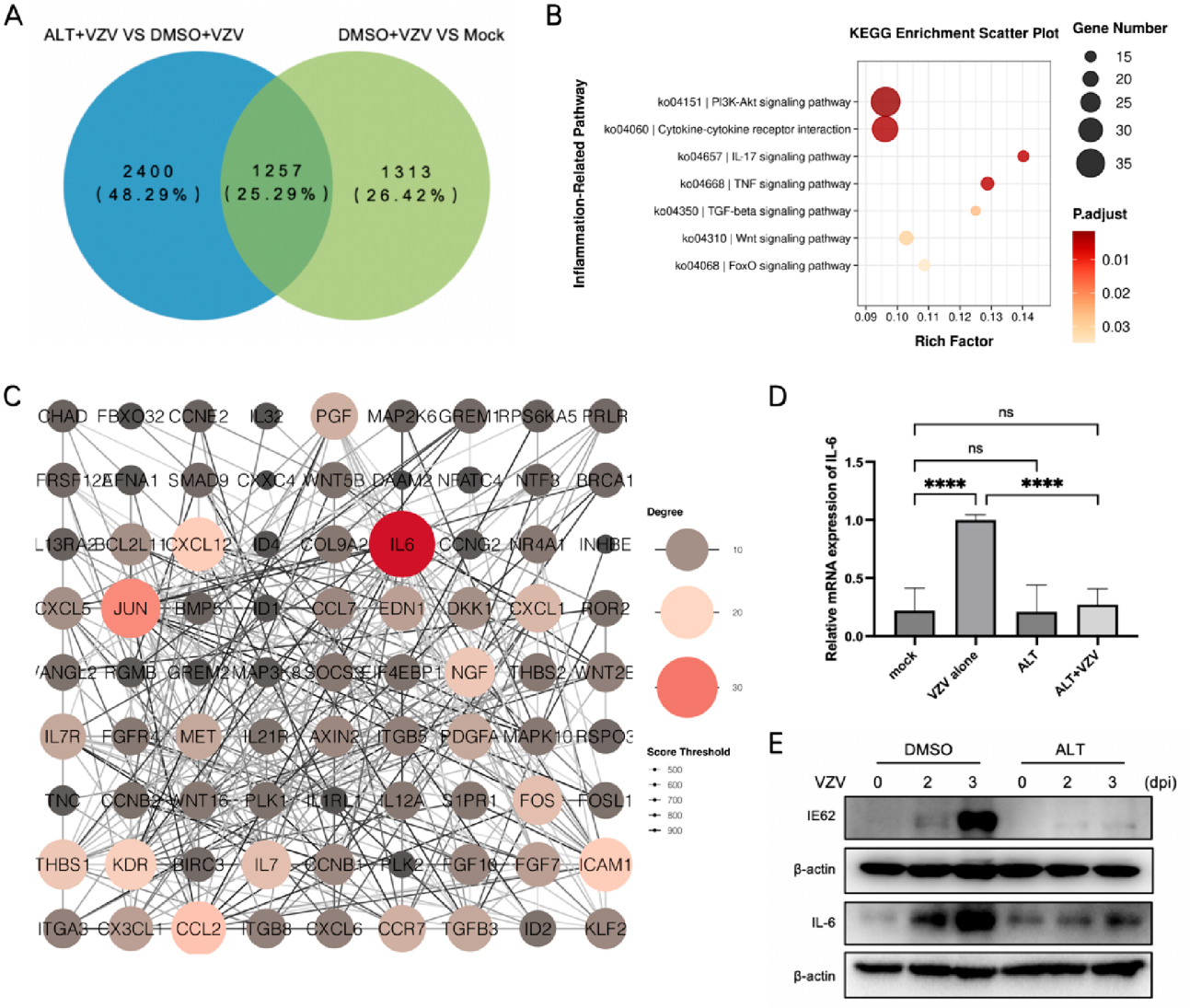

Fig. 4 ALT inhibited VZV-induced IL6 expression in WI-38 cells. (**A**) Venn graph. Differentially expressed genes (DEGs) and overlapped DEGs in Mock, DMSO + VZV and ALT + VZV group. (**B**) Pathways linked to inflammation were revealed via KEGG enrichment analysis of overlapped genes. (**C**) PPI networks identified IL-6 as a hub gene. (**D**) The inhibitory effect of ALT on IL-6 transcriptional level in VZV-infected WI-38 cells. WI-38 cells were infected with VZV at MOI of 0.04 and treated with or without ALT (10μM). Total RNA was isolated at 3dpi and subjected to qPCR analysis ($n = 3$). (**E**) WI-38 cells were inoculated with VZV at MOI of 0.04 and treated with either DMSO or ALT at 10μM. At 0, 2 or 3 days after infection, samples were harvested to analyze the protein levels of IL-6 using Western blotting. The experiment had been repeated three times and one of the typical results was presented. P values were calculated with one-way ANOVA. (****$P < 0.0001$, ns means no significance)

contrast to other cell lines, VZV infection of RPE cells is suitable for obtaining high-titer and cryostable cell-free wild-type VZV stocks that could be used in subsequent plaque inhibition and antiviral susceptibility assays. VZV retinitis (VZVR) is a clinically distinct necrotizing retinitis syndrome caused by VZV that occurs often in immunocompromised patients [47]. RPE cells are susceptible to productive VZV infection and may therefore allow future in *vitro* investigations on the molecular mechanisms of VZV-induced retinitis [36]. Our screening method using ARPE-19 cells to prepare cell-free VZV was suitable for antiviral susceptibility assays and might be instructive in exploring VZVR therapy.

Microscopic observation and plaque assay showed that ALT inhibited the production of VZV progeny virions in a dose-dependent manner at the indicated concentrations (Fig. 1). Further data showed that ALT reduced the expression of VZV lytic genes across multiple temporal cascades (Fig. 2), with consistent effects observed in both ARPE-19 and WI-38 host cells. The VZV gene is known to be expressed in three temporal cascades, designated the immediately early (IE), early(E), and late (L) stages [4, 5]. Among the three phases, IE62 protein, encoded by

ORF62, is an important transcriptional activator of IE, E and L genes [5, 6]; ORF21 is a member of early genes [48], encoding a 115-kd protein located in the nucleocapsid [49]. ORF68 is a member of the class of late genes, encoding the glycoprotein E (gE) [48, 50]. Both ORF21 and ORF68 (encoding gE protein) are necessary for VZV replication [50–52]. Their coordinated downregulation suggested ALT interferes with fundamental processes in the viral life cycle. While VZV gene expression is organized into three temporal cascades, the observed transcriptional suppression likely reflects broader inhibition of viral replication rather than direct transcriptional regulation.

The temporal pattern of ALT's antiviral activity provides insight into potential mechanisms of action. The VZV life cycle consists of the steps of attachment, fusion and uncoating, transcription and replication, budding assembly and envelope acquisition, and release [5]. The significant inhibitory effect of ALT when pretreated cells and added post-infection might indicate that ALT affected different stages during the viral infection cycle (Fig. 3B-C). ALT inhibited the pre-cell group but not the pre-virus group (Fig. 3B-C), indicating that ALT inhibits VZV infection in intracellular viral replication. The antiviral effect of ALT was perhaps more through interactions with cellular components.

To further determine how ALT alleviating VZV infection in vivo, we carried out RNA-sequencing, which showed that ALT regulated multiple inflammatory pathways. Analysis of the PPI network identified the inflammatory cytokine IL6 as a hub gene that might play a central role in the inflammatory response after VZV infection. We found that ALT reduced the VZV-induced elevation of IL6 in the following qPCR and western blotting assay (Fig. 4D-E). IL-6 is a pleiotropic cytokine that is produced in various immune and tissue cells and acts on multiple target cells, thereby promoting both innate and adaptive immune responses at different stages. It can also serve as a marker for the activation of cytokine cascade reactions, reflecting the degree of host inflammatory response [53–56]. Like many viral pathogens, VZV infection is characterized by local inflammatory reactions, which are obvious at the sites of replication in the skin, and proinflammatory cytokines are present in the peripheral blood of infected subjects [57–59]. Patients with HZ (Herpes Zoster) who develop PHN (Postherpetic Neuralgia) have significantly higher levels of IL-6 than those who do not develop PHN, suggesting that the high expression of IL-6 following VZV infection may be associated with the severity of the inflammatory response, which in turn leads to the severity of irreversible nerve damage [59]. In vitro studies had shown that after infection with VZV in human brain vascular adventitial fibroblasts (HBVAFs), human perineural cells (HPNCs), human brain vascular smooth muscle cells (HBVSMCs), and human fetal lung fibroblasts (HFLs), the transcription and expression levels of IL-6 were significantly increased, which led to skin cell stress responses and enhanced the loss of barrier integrity of vascular and perineural cells, facilitating the spread of the virus [60–62]. Varicella and herpes zoster lesions are the direct result of two factors, the destruction of tissue by the virus and the inflammation resulting from the host immune-system responses. ALT can inhibit the increase in IL-6 induced by VZV, likely due to its suppression of VZV replication. However, other studies have found that ALT itself possesses anti-inflammatory properties [63–65]. The topical application of ALT could be an ideal agent to treat both aspects of VZV cutaneous infections.

Abbreviations

VZV	Varicella-zoster virus
ALT	Alantolactone
FOS	Foscarnet
PSGC	PBS-sucrose-glutamate-serum
MOI	Multiplicity of infection
CC50	Half-maximal cytotoxicity concentration
CPE	Cytopathic effects
DEGs	Differentially expressed genes
HZ	Herpes Zoster
PHN	Postherpetic Neuralgia
VZVR	VZV retinitis

Supplementary Information

The online version contains supplementary material available at https://doi.org/10.1186/s12985-025-02759-x.

Supplementary Material 1

Supplementary Material 2

Acknowledgements

We thank Professor Hua Zhu for providing the recombinant VZV.

Author contributions

MGX; LP; WSY and WXN designed the experiments. WXN; KCC; DZY and CYC performed the experiments. WXN analyzed the raw data. WXN wrote the draft. PDL; WSY; MGX critically reviewed the manuscript. All authors read and approved the final manuscript.

Funding

This work was supported by the Projects of Key project joint construction by Science and Technology Department of National Administration of TCM and Zhejiang Administration of TCM (GZY-ZJ-KJ-24055 & GZY-ZJ-KJ-23088), Hangzhou Health Science and Technology Plan (ZD2022005 & A20220018).

Data availability

Data is provided within the manuscript or supplementary information files.

Declarations

Ethics approval and consent to participate

Not applicable.

Consent for publication

All authors approved the manuscript for publication.

Competing interests
The authors declare no competing interests.

Received: 17 November 2024 / Accepted: 22 April 2025
Published online: 09 May 2025

References

1. Manservigi R, Cassai E. The glycoproteins of the human herpesviruses. Comp Immunol Microbiol Infect Dis. 1991;14:81–95.
2. Connolly SA, Jardetzky TS, Longnecker R. The structural basis of herpesvirus entry. Nat Rev Microbiol. 2021;19:110–21.
3. Gershon AA, Breuer J, Cohen JI, Cohrs RJ, Gershon MD, Gilden D, Grose C, Hambleton S, Kennedy PG, Oxman MN, et al. Varicella Zoster virus infection. Nat Rev Dis Primers. 2015;1:15016.
4. Abendroth AMAA. Varicella-Zoster virus. In Fields Virology. Edited by Howley DMKaPM: Lippincott Williams & Wilkins; 2021.
5. Zerboni L, Sen N, Oliver SL, Arvin AM. Molecular mechanisms of varicella Zoster virus pathogenesis. Nat Rev Microbiol. 2014;12:197–210.
6. Cohen JI, Brunell PA, Straus SE, Krause PR. Recent advances in varicella-zoster virus infection. Ann Intern Med. 1999;130:922–32.
7. To KP, Kang SC, Song YJ. The extract of Elaeocarpus sylvestris inhibits human cytomegalovirus immediate early gene expression and replication in vitro. Mol Med Rep. 2014;9:744–8.
8. Cohrs RJ, Badani H, Baird NL, White TM, Sanford B, Gilden D. Induction of varicella Zoster virus DNA replication in dissociated human trigeminal ganglia. J Neurovirol. 2017;23:152–7.
9. Gilden DH, Kleinschmidt-DeMasters BK, LaGuardia JJ, Mahalingam R, Cohrs RJ. Neurologic complications of the reactivation of varicella-zoster virus. N Engl J Med. 2000;342:635–45.
10. Gross GE, Eisert L, Doerr HW, Fickenscher H, Knuf M, Maier P, Maschke M, Müller R, Pleyer U, Schäfer M, et al. S2k guidelines for the diagnosis and treatment of herpes Zoster and postherpetic neuralgia. J Dtsch Dermatol Ges. 2020;18:55–78.
11. Ultsch B, Siedler A, Rieck T, Reinhold T, Krause G, Wichmann O. Herpes Zoster in Germany: quantifying the burden of disease. BMC Infect Dis. 2011;11:173.
12. Kawai K, Gebremeskel BG, Acosta CJ. Systematic review of incidence and complications of herpes Zoster: towards a global perspective. BMJ Open. 2014;4:e004833.
13. Sasivimolphan P, Lipipun V, Likhitwitayawuid K, Takemoto M, Pramyothin P, Hattori M, Shiraki K. Inhibitory activity of Oxyresveratrol on wild-type and drug-resistant varicella-zoster virus replication in vitro. Antiviral Res. 2009;84:95–7.
14. Docherty JJ, Sweet TJ, Bailey E, Faith SA, Booth T. Resveratrol Inhibition of varicella-zoster virus replication in vitro. Antiviral Res. 2006;72:171–7.
15. Gnann JW Jr. Antiviral therapy of varicella-zoster virus infections. In Human Herpesviruses: Biology, Therapy, and Immunoprophylaxis. Edited by Arvin A, Campadelli-Fiume G, Mocarski E, Moore PS, Roizman B, Whitley R, Yamanishi K. Cambridge: Cambridge University Press Copyright © Cambridge University Press; 2007.
16. Ida M, Kageyama S, Sato H, Kamiyama T, Yamamura J, Kurokawa M, Morohashi M, Shiraki K. Emergence of resistance to acyclovir and penciclovir in varicella-zoster virus and genetic analysis of acyclovir-resistant variants. Antiviral Res. 1999;40:155–66.
17. Bao B, Meng Z, Li N, Meng Z, Zhang L, Cao Y, Yao W, Shan M, Ding A. Design, synthesis and antiviral activity studies of schizonepetin derivatives. Int J Mol Sci. 2013;14:17193–203.
18. Bae S, Kim SY, Do MH, Lee CH, Song YJ. 1,2,3,4,6-Penta-O-galloyl-ß-D-glucose, a bioactive compound in Elaeocarpus sylvestris extract, inhibits varicella-zoster virus replication. Antiviral Res. 2017;144:266–72.
19. Kim JE, Song YJ. Anti-varicella-zoster virus activity of cephalotaxine esters in vitro. J Microbiol. 2019;57:74–9.
20. Bae S, Song YJ. Inhibition of varicella–zoster virus replication by an ethanol extract of Lysimachia mauritiana. Mol Med Rep. 2017;15:3847–51.
21. Abu-Galiyun E, Huleihel M, Levy-Ontman O. Antiviral bioactivity of renewable polysaccharides against varicella Zoster. Cell Cycle. 2019;18:3540–9.
22. Zhang Y, Yang B, Tu C, Ping Y, Chen S, Wu T, Zhao Z, Mao Y, Yang Z, Cao Z, et al. Mitochondrial impairment and downregulation of Drp1 phosphorylation underlie the antiproliferative and proapoptotic effects of Alantolactone on oral squamous cell carcinoma cells. J Transl Med. 2023;21:328.
23. Liu X, Bian L, Duan X, Zhuang X, Sui Y, Yang L. Alantolactone: A sesquiterpene lactone with diverse Pharmacological effects. Chem Biol Drug Des. 2021;98:1131–45.
24. Kim M, Song K, Kim YS. Alantolactone improves palmitate-induced glucose intolerance and inflammation in both lean and obese States in vitro: adipocyte and adipocyte-macrophage co-culture system. Int Immunopharmacol. 2017;49:187–94.
25. Gierlikowska B, Gierlikowski W, Demkow U. Alantolactone enhances the phagocytic properties of human macrophages and modulates their Proinflammatory functions. Front Pharmacol. 2020;11:1339.
26. Lim HS, Ha H, Shin HK, Jeong SJ. The Genome-Wide expression profile of Saussurea Lappa extract on house dust Mite-Induced atopic dermatitis in Nc/Nga mice. Mol Cells. 2015;38:765–72.
27. Zhu Y, Ling Y, Wang X. Alantolactone mitigates renal injury induced by diabetes via Inhibition of high glucose-mediated inflammatory response and macrophage infiltration. Immunopharmacol Immunotoxicol. 2020;42:84–92.
28. Yan YY, Zhang Q, Zhang B, Yang B, Lin NM. Active ingredients of Inula helenium L. exhibits similar anti-cancer effects as isoalantolactone in pancreatic cancer cells. Nat Prod Res. 2020;34:2539–44.
29. Wang J, Zhang Y, Liu X, Wang J, Li B, Liu Y, Wang J. Alantolactone enhances gemcitabine sensitivity of lung cancer cells through the reactive oxygen species-mediated Endoplasmic reticulum stress and Akt/GSK3β pathway. Int J Mol Med. 2019;44:1026–38.
30. Zhang J, Shen L, Li X, Song W, Liu Y, Huang L. Nanoformulated codelivery of Quercetin and Alantolactone promotes an antitumor response through synergistic Immunogenic cell death for Microsatellite-Stable colorectal Cancer. ACS Nano. 2019;13:12511–24.
31. Stojanović-Radić Z, Comić L, Radulović N, Blagojević P, Denić M, Miltojević A, Rajković J, Mihajilov-Krstev T. Antistaphylococcal activity of Inula helenium L. root essential oil: Eudesmane sesquiterpene lactones induce cell membrane damage. Eur J Clin Microbiol Infect Dis. 2012;31:1015–25.
32. Seca AM, Grigore A, Pinto DC, Silva AM. The genus Inula and their metabolites: from ethnopharmacological to medicinal uses. J Ethnopharmacol. 2014;154:286–310.
33. Khan M, Yi F, Rasul A, Li T, Wang N, Gao H, Gao R, Ma T. Alantolactone induces apoptosis in glioblastoma cells via GSH depletion, ROS generation, and mitochondrial dysfunction. IUBMB Life. 2012;64:783–94.
34. Wang X, Yu Z, Wang C, Cheng W, Tian X, Huo X, Wang Y, Sun C, Feng L, Xing J, et al. Alantolactone, a natural sesquiterpene lactone, has potent antitumor activity against glioblastoma by targeting IKKβ kinase activity and interrupting NF-κB/COX-2-mediated signaling cascades. J Exp Clin Cancer Res. 2017;36:93.
35. Rezeng C, Yuan D, Long J, Suonan D, Yang F, Li W, Tong L, Jiumei P. Alantolactone exhibited anti-herpes simplex virus 1 (HSV-1) action in vitro. Biosci Trends. 2015;9:420–2.
36. Schmidt-Chanasit J, Bleymehl K, Rabenau HF, Ulrich RG, Cinatl J Jr., Doerr HW. In vitro replication of varicella-zoster virus in human retinal pigment epithelial cells. J Clin Microbiol. 2008;46:2122–4.
37. Sloutskin A, Goldstein RS. Laboratory Preparation of Varicella-Zoster virus: concentration of virus-containing Supernatant, use of a debris fraction and Magnetofection for consistent cell-free VZV infections. J Virol Methods. 2014;206:128–32.
38. Zhang Z, Rowe J, Wang W, Sommer M, Arvin A, Moffat J, Zhu H. Genetic analysis of varicella-zoster virus ORF0 to ORF4 by use of a novel luciferase bacterial artificial chromosome system. J Virol. 2007;81:9024–33.
39. Shakya AK, O'Callaghan DJ, Kim SK. Interferon gamma inhibits Varicella-Zoster virus replication in a cell Line-Dependent manner. J Virol 2019, 93.
40. Luo Z, Kuang X-P, Zhou Q-Q, Yan C-Y, Li W, Gong H-B, Kurihara H, Li W-X, Li Y-F, He R-R. Inhibitory effects of Baicalein against herpes simplex virus type 1. Acta Pharm Sinica B. 2020;10:2323–38.
41. Ma A, Langer J, Hanson KE, Bradley BT. Characterization of the cytopathic effects of Monkeypox virus isolated from clinical specimens and differentiation from common viral exanthems. J Clin Microbiol. 2022;60:e0133622.
42. Kang S, Narazaki M, Metwally H, Kishimoto T. Historical overview of the interleukin-6 family cytokine. J Exp Med 2020, 217.
43. Tanaka T, Narazaki M, Kishimoto T. Interleukin (IL-6) immunotherapy. Cold Spring Harb Perspect Biol 2018, 10.
44. Jassim SA, Naji MA. Novel antiviral agents: a medicinal plant perspective. J Appl Microbiol. 2003;95:412–27.
45. Wang S, Zhou X, He X, Ma S, Sun C, Zhang J, Xu X, Jin W, Yan J, Lin P, Mao G. Suppressive effects of pterostilbene on human cytomegalovirus (HCMV) infection and HCMV-induced cellular senescence. Virol J. 2022;19:224.

46. Grose C, Perrotta DM, Brunell PA, Smith GC. Cell-free varicella-zoster virus in cultured human melanoma cells. J Gen Virol. 1979;43:15–27.
47. Moorthy RS, Weinberg DV, Teich SA, Berger BB, Minturn JT, Kumar S, Rao NA, Fowell SM, Loose IA, Jampol LM. Management of varicella Zoster virus retinitis in AIDS. Br J Ophthalmol. 1997;81:189–94.
48. Rahaus M, Desloges N, Wolff MH. Development of a multiplex RT-PCR to detect transcription of varicella-zoster virus encoded genes. J Virol Methods. 2003;107:257–60.
49. Mahalingam R, Lasher R, Wellish M, Cohrs RJ, Gilden DH. Localization of varicella-zoster virus gene 21 protein in virus-infected cells in culture. J Virol. 1998;72:6832–7.
50. Montalvo EA, Parmley RT, Grose C. Structural analysis of the varicella-zoster virus gp98-gp62 complex: posttranslational addition of N-linked and O-linked oligosaccharide moieties. J Virol. 1985;53:761–70.
51. Berarducci B, Rajamani J, Zerboni L, Che X, Sommer M, Arvin AM. Functions of the unique N-terminal region of glycoprotein E in the pathogenesis of varicella-zoster virus infection. Proc Natl Acad Sci U S A. 2010;107:282–7.
52. Xia D, Srinivas S, Sato H, Pesnicak L, Straus SE, Cohen JI. Varicella-zoster virus open reading frame 21, which is expressed during latency, is essential for virus replication but dispensable for establishment of latency. J Virol. 2003;77:1211–8.
53. Hagihara K, Nishikawa T, Isobe T, Song J, Sugamata Y, Yoshizaki K. IL-6 plays a critical role in the synergistic induction of human serum amyloid A (SAA) gene when stimulated with Proinflammatory cytokines as analyzed with an SAA isoform real-time quantitative RT-PCR assay system. Biochem Biophys Res Commun. 2004;314:363–9.
54. Hunter CA, Jones SA. IL-6 as a keystone cytokine in health and disease. Nat Immunol. 2015;16:448–57.
55. Mihara M, Hashizume M, Yoshida H, Suzuki M, Shiina M. IL-6/IL-6 receptor system and its role in physiological and pathological conditions. Clin Sci (Lond). 2012;122:143–59.
56. Tanaka T, Narazaki M, Kishimoto T. IL-6 in inflammation, immunity, and disease. Cold Spring Harb Perspect Biol. 2014;6:a016295.
57. Bruder E, Ersch J, Hebisch G, Ehrbar T, Klimkait T, Stallmach T. Fetal varicella syndrome: disruption of neural development and persistent inflammation of non-neural tissues. Virchows Arch. 2000;437:440–4.
58. Shaikh S, Ta CN. Evaluation and management of herpes Zoster ophthalmicus. Am Fam Physician. 2002;66:1723–30.
59. Zhu SM, Liu YM, An ED, Chen QL. Influence of systemic immune and cytokine responses during the acute phase of Zoster on the development of postherpetic neuralgia. J Zhejiang Univ Sci B. 2009;10:625–30.
60. Jones D, Neff CP, Palmer BE, Stenmark K, Nagel MA. Varicella Zoster virus-infected cerebrovascular cells produce a Proinflammatory environment. Neurol Neuroimmunol Neuroinflamm. 2017;4:e382.
61. Jarosinski KW, Carpenter JE, Buckingham EM, Jackson W, Knudtson K, Moffat JF, Kita H, Grose C. Cellular stress response to Varicella-Zoster virus infection of human skin includes highly elevated Interleukin-6 expression. Open Forum Infect Dis. 2018;5:ofy118.
62. Blackmon AM, Como CN, Bubak AN, Mescher T, Jones D, Nagel MA. Varicella Zoster virus alters expression of cell adhesion proteins in human perineurial cells via Interleukin 6. J Infect Dis. 2019;220:1453–61.
63. Kim M, Song K, Kim YS. Alantolactone improves prolonged exposure of Interleukin-6-Induced skeletal muscle inflammation associated glucose intolerance and insulin resistance. Front Pharmacol. 2017;8:405.
64. Dang X, He B, Ning Q, Liu Y, Guo J, Niu G, Chen M. Alantolactone suppresses inflammation, apoptosis and oxidative stress in cigarette smoke-induced human bronchial epithelial cells through activation of Nrf2/HO-1 and Inhibition of the NF-κB pathways. Respir Res. 2020;21:95.
65. Wang J, Jiang Y, Jin L, Qian C, Zuo W, Lin J, Xie L, Jin B, Zhao Y, Huang L, Wang Y. Alantolactone attenuates high-fat diet-induced inflammation and oxidative stress in non-alcoholic fatty liver disease. Nutr Diabetes. 2024;14:41.

Publisher's note